opening the prospect of atomic optical clocks operating at vacuum-ultraviolet or extreme-ultraviolet frequencies. Outside frequency metrology, amplified frequency combs could be used to perform quantum control experiments on a time scale much longer than is currently possible, because phase coherence can be maintained for many consecutive laser pulses.

References and Notes

1. R. Holzwarth *et al.*, *Phys. Rev. Lett.* **85**, 2264 (2000).
2. D. J. Jones *et al.*, *Science* **288**, 635 (2000).
3. Th. Udem, R. Holzwarth, T. W. Hänsch, *Nature* **416**, 233 (2002).
4. M. Niering *et al.*, *Phys. Rev. Lett.* **84**, 5496 (2000).
5. Th. Udem *et al.*, *Phys. Rev. Lett.* **86**, 4996 (2001).
6. M. Fischer *et al.*, *Phys. Rev. Lett.* **92**, 230002 (2004).
7. J. P. Uzan, *Rev. Mod. Phys.* **75**, 403 (2003).
8. N. F. Ramsey, *Phys. Rev.* **76**, 996 (1949).
9. A. Clairon, C. Salomon, S. Guellati, W. D. Phillips, *Europhys. Lett.* **16**, 165 (1991).
10. M. M. Salour, C. Cohen-Tannoudji, *Phys. Rev. Lett.* **38**, 757 (1977).
11. M. M. Salour, *Rev. Mod. Phys.* **50**, 667 (1978).
12. R. Teets, J. N. Eckstein, T. W. Hänsch, *Phys. Rev. Lett.* **38**, 760 (1977).
13. M. Bellini, A. Bartoli, T. W. Hänsch, *Opt. Lett.* **22**, 540 (1997).
14. M. J. Snadden, A. S. Bell, E. Riis, A. I. Ferguson, *Opt. Commun.* **125**, 70 (1996).
15. A. Baltuška *et al.*, *Nature* **421**, 611 (2003).
16. J. N. Eckstein, A. I. Ferguson, T. W. Hänsch, *Phys. Rev. Lett.* **40**, 847 (1978).
17. A. Marian, M. C. Stowe, J. R. Lawall, D. Felinto, J. Ye, *Science* **306**, 2063 (2004); published online 18 November 2004 (10.1126/science.1105660).
18. R. Zerne *et al.*, *Phys. Rev. Lett.* **79**, 1006 (1997).
19. S. Cavalieri, R. Eramo, M. Materazzi, C. Corsi, M. Bellini, *Phys. Rev. Lett.* **89**, 133002 (2002).
20. K. S. E. Eikema, W. Ubachs, W. Vassen, W. Hogervorst, *Phys. Rev. A* **55**, 1866 (1997).
21. S. D. Bergeson *et al.*, *Phys. Rev. Lett.* **80**, 3475 (1998).
22. A. Apolonski *et al.*, *Phys. Rev. Lett.* **85**, 740 (2000).
23. S. Witte, R. Th. Zinkstok, W. Hogervorst, K. S. E. Eikema, *Appl. Phys. B* **78**, 5 (2004).
24. Standard amplifiers operate in saturated mode to reduce output power fluctuations and can therefore amplify only one pulse. In the present experiment, the number of pulses that can be amplified is limited to three by the EOM, which must be switched off before any backreflections from the amplifier lead to uncontrolled extra pulses. An additional Faraday isolator in the setup would lift this limitation.
25. An EOM and polarizing optics were used to project the interference patterns for two consecutive pulses simultaneously and vertically displaced from one another on a CCD camera. The relative positions on the CCD (up or down) were alternated by switching the EOM; the relative phase shift to the comb laser was then determined by looking at the phase difference in both projection situations, so as to cancel out any alignment effects.
26. The Doppler shift can in principle be reduced on a two-photon transition by measuring with colliding pulses from opposite sides. This arrangement also enhances the signal, as was seen experimentally. However, contrary to CW spectroscopy, Doppler-free signal (photons absorbed from opposite sides) and Doppler-shifted signal (two photons from one side) cannot be distinguished properly in the case of excitation with two ultrashort pulses, because the large bandwidth always contains a resonant frequency. This situation might lead to a calibration error when there is an imbalance in signal strength from opposite sides. Another aspect is that the total Doppler shift has an ambiguity due to the periodicity of the signal. The difference in Doppler shift for the isotopes, which is on the order of a few hundred kHz, therefore provides a valuable initial estimate of about 25 MHz for this shift. From the measurement of the absolute positions, one can then determine the Doppler shift to be 29 MHz for each of the counterpropagating beams.
27. The energy ratio of pulses 1, 2, and 3 is 1.0:0.91:0.6. In all measurements with two pulses, the pulse energies have been kept equal to within about 5%.
28. V. Kaufman, *J. Res. Natl. Inst. Stand. Technol.* **98**, 717 (1993).
29. F. Brandi, W. Hogervorst, W. Ubachs, *J. Phys. B* **35**, 1071 (2002).
30. Two systematic effects dominate the determination of the resonance frequency: the phase shifts induced by the amplifier (100 to 200 mrad in the infrared), and the residual Doppler shift (2 MHz) due to possible misalignment of the counterpropagating beams. Other effects include light-shifts (0.47 ± 0.44 MHz), static field effects ($\ll$100 kHz), the second-order Doppler shift ($\sim$1 kHz), and a recoil shift (209 kHz). The phase shift due to the pulse-picker EOM is negligible ($<$5 mrad) when it is aligned such that it acts as a pure polarization rotator, as verified experimentally. The phase shift due to frequency doubling is negligible as well, on the order of 1 mrad in the ultraviolet, as estimated from the model of (*31*).
31. R. DeSalvo *et al.*, *Opt. Lett.* **17**, 28 (1992).

32. Supported by the Foundation for Fundamental Research on Matter (FOM), the Netherlands Organization for Scientific Research (NWO), the EU Integrated Initiative FP6 program, and the Vrije Universiteit Amsterdam.

21 October 2004; accepted 30 November 2004
10.1126/science.1106612

Charging Effects on Bonding and Catalyzed Oxidation of CO on Au_8 Clusters on MgO

Bokwon Yoon,[1] Hannu Häkkinen,[1]* Uzi Landman,[1]† Anke S. Wörz,[2] Jean-Marie Antonietti,[2] Stéphane Abbet,[2] Ken Judai,[2] Ueli Heiz[2]†

Gold octamers (Au_8) bound to oxygen-vacancy F-center defects on Mg(001) are the smallest clusters to catalyze the low-temperature oxidation of CO to CO_2, whereas clusters deposited on close-to-perfect magnesia surfaces remain chemically inert. Charging of the supported clusters plays a key role in promoting their chemical activity. Infrared measurements of the stretch vibration of CO adsorbed on mass-selected gold octamers soft-landed on MgO(001) with coadsorbed O_2 show a red shift on an F-center–rich surface with respect to the perfect surface. The experiments agree with quantum ab initio calculations that predict that a red shift of the C–O vibration should arise via electron back-donation to the CO antibonding orbital.

The exceptional catalytic properties of small gold aggregates (*1*, *2*) have motivated research (*3*–*17*) aimed at providing insights into the molecular origins of this unexpected reactivity of gold. Investigations on size-selected small gold clusters, $Au_n (2 \leq n \leq 20)$, soft-landed on a well-characterized metal oxide support [specifically, a MgO(001) surface with and without oxygen vacancies or F centers], revealed (*4*) that gold octamers bound to F centers of the magnesia surface are the smallest known gold heterogeneous catalysts that can oxidize CO into CO_2 at temperatures as low as 140 K. The same cluster bound to a MgO surface without oxygen vacancies is catalytically inactive for CO combustion (*4*).

Quantum-mechanical ab initio simulations, in juxtaposition with laboratory experiments, led us to conclude (*4*, *5*) that the key for low-temperature gold catalysis in CO oxidation is the binding of O_2 and CO to the supported gold nanocluster, which activates the O–O bond to a peroxo-like (or superoxo-like) adsorbate state. This process is enabled by resonances between the cluster's electronic states and the $2\pi^*$ antibonding states of O_2, which are pulled below the Fermi level (E_F). Charging of the metal cluster, caused by partial transfer of charge from the substrate F center into the deposited cluster, underlies the catalytic activity of the gold octamers (Au_8), as well as that of other small gold clusters (Au_n, $8 \leq n \leq 20$) (*4*). These investigations predicted that (i) the F centers on the metal oxide support surface play the role of active sites (a concept that has been central to the development of heterogeneous catalysis); (ii) these sites serve to anchor the deposited clusters more strongly than sites on the undefective surface (thus inhibiting their migration and coalescence); and, most important, (iii) these active sites control the charge state of the gold clusters, thus promoting the activation of adsorbed reactant molecules (that is, formation of the aforementioned peroxo or superoxo species) (*18*).

We have studied the cluster-charging propensity of the F-center active sites, both exper-

[1]School of Physics, Georgia Institute of Technology, Atlanta, GA 30332–0430, USA. [2]Departement Chemie, Lehrstuhl für Physikalische Chemie I, Technische Universität München, Lichtenbergstraße 4, 85747 Garching, Germany.

*Present address: Department of Physics, Nanoscience Center, Box 35, FIN-40014, University of Jyväskyla, Finland.

†To whom correspondence should be addressed. E-mail: uzi.landman@physics.gatech.edu (U.L.); ulrich.heiz@ch.tum.de (U.H.)

imentally and theoretically, by examining the vibrational properties of adsorbed CO. The internal CO stretch frequency ν(CO), measured in the presence of coadsorbed O_2 for the octamer bound to the F center of the magnesia substrate [Au_8/CO/O_2/MgO(FC)], shifted to lower frequency by about 25 to 50 cm^{-1} compared to the ν(CO) frequency recorded for the gold octamer bound to the F-center–free MgO(001) surface (Au_8/CO/O_2/MgO). Systematic ab initio calculations (*4*, *5*) reveal that this shift is caused by enhanced back-donation (from the gold nanocluster) into the antibonding 2π* orbital of the CO adsorbed on the cluster anchored to a surface F center. In addition, calculations addressing free Au_8/O_2/CO coadsorption complexes provide further evidence that the bonding characteristics and spectral shifts are related to each other and that they are correlated with, and sensitive to, the charge state of the cluster (*18*).

We reproduced experimentally the results of our earlier investigations pertaining to the enhanced catalytic activity of Au_8 clusters deposited on F-center–defective MgO surfaces, and then went beyond those measurements by recording (under the same conditions as for the reactivity studies) the infrared (IR) spectra of the reactants as a function of the annealing temperature (Fig. 1). Size-selected Au_8 cations were deposited at 90 K, with low kinetic energy, onto MgO(FC) thin films at low coverages (8×10^{12} clusters/cm^2). Several experimental studies [such as the synthesis of monodispersed model catalysts by using soft-landing cluster deposition (*19*)] have shown that, in general, upon deposition, the clusters are neutralized, maintain their nuclearity, and stay well isolated at defect sites. These model catalysts were then saturated with isotopicaly labeled $^{18}O_2$ and $^{13}C^{16}O$; the order of the exposure of the reactants (0.2 Langmuir) did not change the activity (unlike the case for other metals). Upon heating, $^{13}C^{16}O^{18}O$ was produced at 140 and 280 K, as shown in Fig. 1A. No other isotopomer was detected, indicating that only the adsorbed O_2 and CO participate in the reaction. We attribute the reaction at 140 K to an ensemble of Au_8 clusters, with O_2 bound to the top facet of the cluster; and the reaction at 280 K to an Au_8 ensemble, with O_2 bound to the perimeter of the cluster at the cluster-to-substrate interface (Fig. 2B). These assignments were made by us previously (*4*) on the basis of calculated activation barriers for the CO oxidation. Specifically for small gold clusters, only a single O_2 molecule can be adsorbed, and thus the two ensembles are saturated with O_2 via either direct adsorption or reverse spillover.

The corresponding IR study reveals absorption bands of the two reactants. In Fig. 1, C and D, we show only the spectra for adsorbed CO, with the decrease in intensity correlating with the formation of CO_2 (Fig. 1C). The IR band corresponding to adsorbed O_2 occurs around 1300 cm^{-1} for both the F-center–rich and perfect MgO surfaces. The IR frequencies (2049 and 2077 cm^{-1}) are typical for on-top adsorbed ^{13}CO on gold. In this context, we recall that the band at 2127 cm^{-1} originates from ^{13}CO adsorbed directly on defect sites of the MgO(001) surface (*20*). On Au single crystals (*21*–*23*), as well as on oxide-supported Au particles (*9*, *24*, *25*), sharp ^{13}CO absorption bands occur at a single frequency around 2060 cm^{-1}. We infer that the detection of two absorption features reveals the presence of (at least) two types of adsorbed CO molecules, which differ somewhat in how they bind to the Au_8 cluster (Fig. 2C and discussion below).

Upon heating, the population of the three bands changes. At an annealing temperature of 220 K (subsequent to the 140 K combustion reaction), a small single absorption band at 2055 cm^{-1} was observed (Fig. 1C). Earlier studies (*26*) detected such a band for ^{13}CO adsorbed to Au_8/MgO(FC).

In contrast to the above, gold octamers adsorbed on an F-center–free MgO(001) surface were essentially inactive for the combustion reaction (Fig. 1B). In fact, even under quasi–steady-state conditions with pulsed molecular beams, no CO_2 formation was observed. The absorption band of ^{13}CO in this case (2102 cm^{-1}) was shifted to a higher frequency (by 25 to 50 cm^{-1}), as compared to the case of ^{13}CO adsorbed on a gold octamer deposited on MgO(FC).

The above-noted red shift of the CO stretch when the molecule is adsorbed on Au_8 supported on MgO(001)(FC) is a key for elucidating the change in the charge state of the gold octamer bound to F-center defects on the MgO surface. The absorption frequency of CO adsorbed on metal surfaces depends strongly on the population of the 2π* orbital, because occupation of this antibonding orbital weakens the C–O bond. Furthermore, results from extensive ab initio calculations, using the method developed in

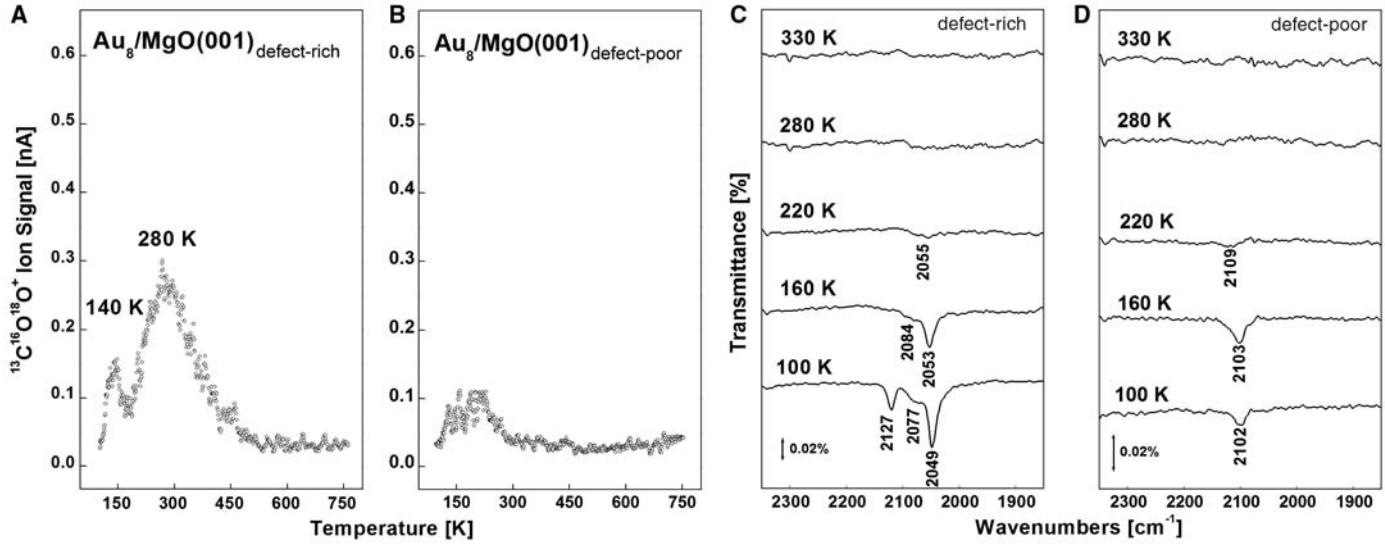

Fig. 1. Mass spectrometric signals pertaining to the formation of CO_2 on Au_8 deposited on (**A**) F-center–rich and (**B**) F-center–free MgO(001) thin films. To unambiguously show that both CO and O_2 are involved in the reaction, isotopically labeled ^{13}CO and $^{18}O_2$ were used. [(**C**) and (**D**)] Fourier-transform IR spectra measured for the same surfaces (defect-rich and defect-poor) and with the same CO and O_2 exposures as in (A) and (B), respectively, at various annealing temperatures. The indicated temperatures cannot be compared directly with the ones in the temperature-programmed reaction spectrum but are lower limits. We have also observed an IR absorption band at 1300 cm^{-1}, which we attribute to superoxo/peroxo-type O_2. In order to better disentangle the vibrational band of ^{13}CO adsorbed on Au_8 deposited on defect-poor films (B) from that of the CO weakly bound to the support material, the sample was annealed to 120 K. In this way, the ^{13}CO frequency from MgO-adsorbed CO disappears, otherwise observed at 2127 cm^{-1}.

(*27*) [see also (*18*)], given in Table 1 for the isolated $Au_8/O_2/^{13}CO$ complex (which we present first in order to allow a clear distinction between charging and other support-related effects), reveal that the ^{13}CO stretch vibration shifts to lower frequency in a manner that is correlated with increased charging of the complex (given by Q_c in Table 1), as well as with the estimated increase in the population of the antibonding state [given by δQ(CO) in Table 1]. For a neutral free complex with zero spin [$Q_c = 0$ and $S = 0$ in Table 1; see the corresponding atomic configuration shown in the inset of Fig. 2], a vibrational frequency of 2009 cm^{-1} was obtained for the adsorbed ^{13}CO molecule. We attribute the calculated decrease in frequency (61 cm^{-1}) in comparison to the value calculated for the free molecule (2070 cm^{-1}) to a net excess charge [$\delta Q(CO) = 0.28e$, where e is the electron charge] on the adsorbed molecule. The excess charge on the molecule results from back-donation into the CO($2\pi^*$) antibonding state.

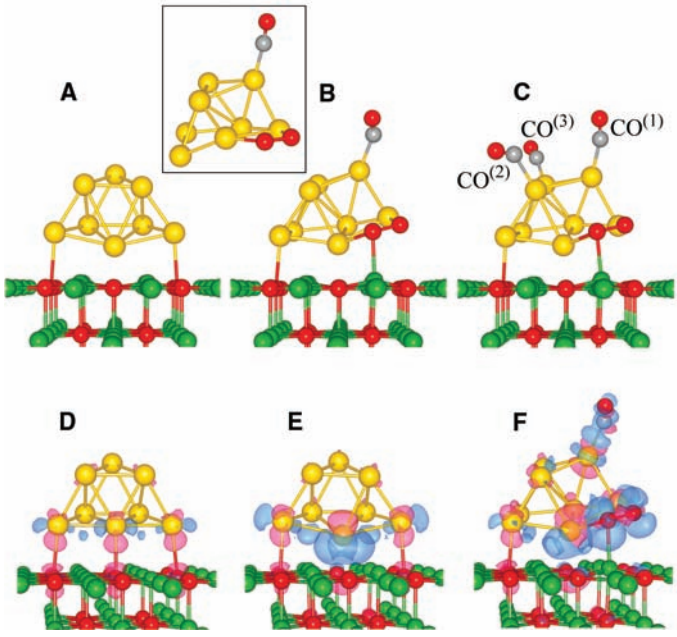

Fig. 2. Optimized configurations of (**A**) a bare Au_8 cluster (yellow spheres) adsorbed on an F center of a MgO(001) surface (O atoms are in red and Mg atoms in green) and (**B**) a surface-supported gold octamer with O_2 adsorbed at the interface between the Au_8 cluster and the magnesia surface and a CO molecule adsorbed on the top triangular facet (the C atom is depicted in gray). There is a significant change in the geometry of Au_8 compared to the one shown in (A). The inset between (A) and (B) shows a local-energy-minimum structure of the free Au_8 cluster in the three-dimensional (3D) isomeric form with coadsorbed O_2 and CO molecules. Although in the global ground state of the free $Au_8/O_2/CO$ complex the gold octamer is characterized by a higher degree of 2D character (*14*), we chose to display here an isomer that closely resembles the structure of the surface-adsorbed complex: Compare the structure in the inset with that shown in (B). (**C**) Au_8 on the magnesia surface [MgO(FC)] with three CO molecules adsorbed on the top facet of the cluster and an O_2 molecule preadsorbed at the interface between the cluster and the magnesia surface. The molecule marked $CO^{(2)}$ lies parallel to the surface and is thus not IR-active in the experimental configuration used here. The C–O bond length $d(CO^{(i)})$, the charge transferred to the $CO^{(i)}$ molecule $\Delta Q^{(i)}$, and the calculated C–O vibrational frequency $\nu^{(i)}$ (i =1, 2, and 3), as well as the corresponding values for the O_2 molecule, are as follows: $d(CO^{(i)})$ [Å] = 1.151, 1.158, 1.153; $d(O_2)$ = 1.422; $\delta Q^{(i)}$ [e] = 0.31, 035, 0.32; $\delta Q(O_2)$ [e] = 1.12; $\nu^{(i)}$ [cm^{-1}] = 1993, 1896, 1979. Isosurfaces of charge differences are as follows: (**D**) Au_8 cluster adsorbed on defect-free MgO, $\delta\rho = \rho_{tot} - (\rho_{Au8} + \rho_{MgO})$, where $\rho_{tot} = \rho[Au_8/MgO]$; (**E**) Au_8 cluster anchored to a surface F center of MgO, $\delta\rho = \rho_{tot} - (\rho_{Au8} + \rho_{MgO(FC)})$, where $\rho_{tot} = \rho[Au_8/MgO(FC)]$; (**F**) same as (E) but with O_2 and CO molecules adsorbed on the gold cluster, $\delta\rho = \rho_{tot} - (\rho_{Au8} + \rho_{O2} + \rho_{CO} + \rho_{MgO(FC)})$, where $\rho_{tot} = \rho[Au_8/O_2/CO/MgO(FC)]$. Pink isosurfaces represent $\delta\rho < 0$ (depletion) and blue ones correspond to $\delta\rho > 0$ (excess). All of the isosurfaces are plotted for the same (absolute) value of the density difference ($\delta\rho$) in order to allow direct comparison between the different cases.

Table 1. Results for free $Au_8/O_2/^{13}CO$ complexes as a function of the amount of excess electron charging Q_c, shown for various values of the spin. For the neutral cluster ($Q_c = 0$), we show the triplet ($S = 1$) and singlet ($S = 0$) states. The quantities that we display are: $\nu(^{13}CO)$, the ^{13}CO vibrational frequency; the calculated excess electronic charge on the adsorbed molecules δQ(CO) and $\delta Q(O_2)$, with the procedure used for achieving these estimates described in (*18*); and the bond distances d(CO) and $d(O_2)$. The calculated values for the isolated molecules are d(CO) = 1.14 Å and $d(O_2)$ = 1.24 Å, compared to the gas-phase experimental values of 1.13 and 1.21 Å, respectively. The calculated vibrational frequency of gas-phase ^{13}CO is 2070 cm^{-1}, which is 25 cm^{-1} smaller than the experimental value $\nu_{exp}(^{13}CO)$ = 2095 cm^{-1}.

Q_c (e)	S	ν (cm^{-1})	$d(^{13}CO)$ (Å)	δQ(CO) (e)	$d(O_2)$ (Å)	$\delta Q(O_2)$ (e)
0	1	2005	1.149	0.29	1.336	0.71
0.25	0.875	1987	1.150	0.32	1.344	0.75
0.5	0.75	1968	1.154	0.35	1.350	0.77
1.0	0.5	1926	1.160	0.43	1.364	0.86
0	0	2009	1.148	0.28	1.378	0.88
0.25	0	1990	1.150	0.31	1.381	0.89
0.5	0	1975	1.153	0.34	1.385	0.92
1.0	0	1920	1.158	0.41	1.398	1.00

As expected, such donation of charge from occupied orbitals of the metal to unoccupied states of the adsorbed molecule is even more pronounced (0.88e) for the more electronegative O_2 molecule. Upon charging the complex with up to 1.0e, the net excess charge on the ^{13}CO molecule increases to 0.41e, and the CO stretch redshifts by 89 cm^{-1} to 1920 cm^{-1}. The increased degree of charging of the metal cluster with back-donation, and the consequent decrease of ν(CO), increase the C–O bond length from 1.148 Å for Q_c = 0 to 1.158 Å for Q_c = 1.0e. Similar changes were seen starting from the triplet state of the neutral complex (Table 1).

We next focused on the adsorption of CO to gold complexes surface-supported on perfect or defective magnesia [with an oxygen molecule preadsorbed at the interface between the cluster periphery and the MgO surface (Fig. 2B)]; that is, $Au_8/O_2/MgO$ or $Au_8/O_2/MgO(FC)$. Three energy-optimized deposited cluster configurations pertinent to the experimental work are displayed in the top row of Fig. 2, A to C. The bare adsorbed Au_8 cluster (Fig. 2A) exhibits only a slight distortion from the structure of the corresponding gas-phase neutral cluster (*4*, *5*), consisting mainly of a displacement of the gold atom of the cluster closest to the surface oxygen vacancy. The cluster is anchored strongly to the defective MgO surface (with a binding energy of 3.44 eV) compared to a significantly weaker binding to the defect-free surface (1.22 eV). From examination of the charge-difference isosurfaces displayed in Fig. 2, we observe that bonding of the Au_8 cluster to the MgO(FC) surface is accompanied by a significantly larger degree of charge transfer from the magnesia surface to the gold cluster (Fig. 2E) as compared to the case of adsorption on an F-center–free surface (Fig. 2D).

Optimal geometries with a single adsorbed CO molecule, $Au_8/O_2/CO/MgO(FC)$, and at saturation coverage of the cluster [that is, with three adsorbed CO molecules, $Au_8/O_2/(CO)_3/MgO(FC)$] are shown in Fig. 2, B and C, respectively. Comparison between the bare-cluster geometry in Fig. 2A with those shown in Fig. 2, B and C, reveals a significant change

in the geometry of the gold cluster caused by the adsorption of the reactant molecules, mainly the peripherially adsorbed O_2. This structural change, occurring during adsorption (or in the course of reaction), is a manifestation of the "structural fluxtionality" of clusters (*5*). The system shown in Fig. 2C possesses two IR-active ^{13}CO molecules ($CO^{(1)}$ and $CO^{(3)}$), as we had seen experimentally (*18*).

Because the bonding characteristics, and other properties of the system, with a single adsorbed CO molecule (Fig. 2B) are similar to the ones associated with the CO-saturated cluster (Fig. 2C), we focus next on the former (which is more convenient to analyze and illustrate). The energetics of the adsorption of the O_2 and CO molecules to the defect-free and F-center clusters, corresponding in each case to two possible spin states (S = 0 or 1), together with the calculated amount of charge transferred to the deposited complex (gold cluster and adsorbed molecules), the bond length d(CO), and the calculated vibrational frequency are given in Table 2. Stronger binding of O_2 to the cluster occurs in the presence of the F center (A and B in Table 2).

Adsorption is accompanied by a significant degree of charge transfer, which in the case of the defective surface is directed from the oxygen vacancy into the deposited gold cluster and adsorbed molecules. Comparison of the charge-difference isosurfaces for the bare cluster (Fig. 2E) and for the cluster with adsorbed O_2 and CO molecules (Fig. 2F), bonded to MgO(FC), reveals a significant amount of charge excess on the adsorbed molecules. The consequent weakening of intramolecular bonds manifests itself in increased bond lengths and lower vibrational frequencies of the adsorbed molecules (Table 2) (*28*).

The correlation diagram (Fig. 3, A to C) depicts the local density of states (LDOS) for the two reactants, CO (Fig. 3A) and the Au_8/O_2/MgO(FC) complex (Fig. 3C), as well as for the product complex Au_8/O_2/CO/MgO(FC) with the CO adsorbed on the deposited cluster (Fig. 3B). The LDOS of Au_8/O_2/CO/MgO(FC) is reproduced in Fig. 4 along with images of the corresponding molecular orbitals, which aid visualization of the bonding mechanism discussed below. As expected, the 3σ and the nonbonding 4σ (oxygen lone-pair) molecular orbitals of the isolated CO are not involved in the bonding to the cluster complex, and the nonbonding 5σ (carbon lone-pair) orbital is stabilized by the interaction (by about 3eV) and thus it contributes to CO chemisorption (*29*). The 1π level is slightly pushed upward in energy (<1eV).

The LDOS of the complex projected on the adsorbed CO also reveals contributions of the 2π* orbitals that are spread over the entire energy range of the cluster's electronically occupied spectrum (Fig. 3B, the black-shaded LDOS for energies between about –10eV and E_F). The 2π* orbitals of the CO molecule are pushed below E_F, which populates this state via back-donation [that is,

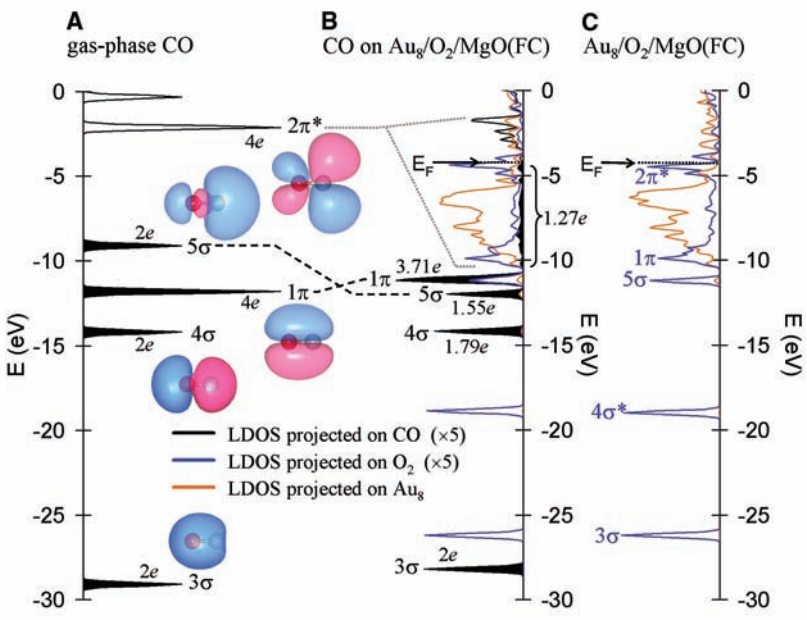

Fig. 3. LDOS correlation diagram of (**A**) free CO, (**C**) Au_8/O_2/MgO(FC), and (**B**) after adsorption of a CO molecule, resulting in the complex Au_8/O_2/CO/MgO(FC). The results correspond to the spin singlet (S = 0) case. The electron populations of the various levels of the free and adsorbed CO molecule are given as 2*e*, 4*e*, etc., and isosurface images of the orbitals of the free CO molecules are also shown in (A). Black dashed lines indicate orbital shifts and redistribution caused by the adsorption of the CO molecule.

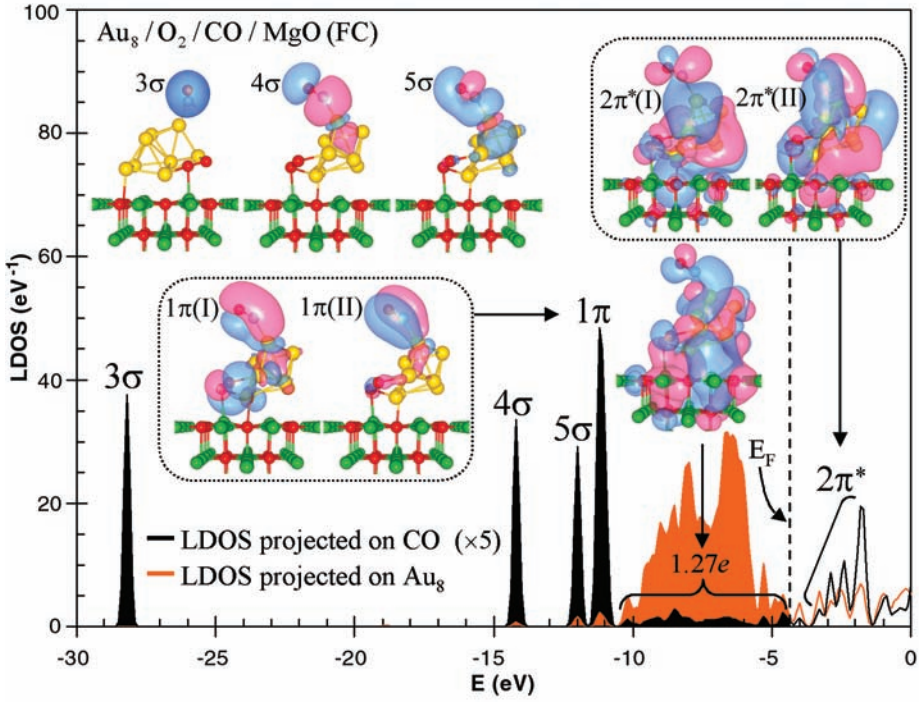

Fig. 4. LDOS and orbitals of the Au_8/O_2/CO complex adsorbed on MgO(FC). Results are shown for the spin singlet S = 0 case. The LDOS projected on the CO molecule is shown in black and that projected on the gold cluster is colored orange. E_F is indicated by a dashed line. The electronic population of the orbitals of the CO molecule (found to be mainly of 2π* character), with energies in the range that overlaps the gold cluster states, provides an estimate of the back-donated charge (1.27*e*). Included also are isosurface images of the wave functions of the Au_8/O_2/CO/MgO(FC) complex, which may be identified with the indicated orbitals of CO (compare to the orbital images of the free CO molecule in Fig. 3A).

Table 2. Binding energies: BE(O_2), binding energy of O_2 to Au_8/MgO; BE(CO), binding energy of CO to Au_8/O_2/MgO. Excess electronic charge $\Delta Q(Au_8/O_2/CO)$ on the complex adsorbed on the (001) surface of magnesia is shown. The C–O bond length d(CO) and the C–O stretch vibrational frequency $\nu(^{13}CO)$ are shown. Results are given for the gold octamer adsorbed on a MgO(001) surface with (F center), or without (F-center–free), a surface F center, and in each case we give results calculated for two spin states, S. The calculated amount of charge transferred to a bare gold octamer cluster adsorbed on the defect-free surface is $\Delta Q(Au_8/MgO) = 0.82e$, and it is significantly larger for the cluster adsorbed on a surface F center; that is, $\Delta Q(Au_8/MgO(FC)) = 1.44e$. The excess charge ΔQ is calculated as described in (*18*).

	S	BE(O_2) (eV)	BE(CO) (eV)	$\Delta Q(Au_8/O_2/CO)$ (e)	d(CO) (Å)	ν (^{13}CO) (cm^{-1})
				F center		
A	1	0.33	0.79	1.52	1.155	1937
B	0	0.47	0.65	1.58	1.156	1931
				F-center–free		
C	1	0.30	0.79	0.87	1.152	1965
D	0	0.15	0.91	1.01	1.150	1994

hybridization and population of the initially unoccupied antibonding orbitals of the CO molecule through interaction with occupied surface orbitals (*30*–*32*)]. All of these features are also present in the correlation diagram of the cluster complex bound to the defect-free MgO surface (not shown here), where back-donation, however, is less pronounced. We can estimate the amount of back-donated electronic charge by integrating over the squared amplitude of the $2\pi^*$ orbital located below E_F. For the Au_8/O_2/CO bound to the F center of the MgO support, 1.27e are back-donated into the $2\pi^*$ orbital, whereas a smaller degree of back-donation (1.18e) occurs for the complex bound to the undefective surface.

The above-noted difference in the degree of back-donation is manifested in a variation of the stretch frequencies of the adsorbed CO molecules, and these correlate with the aforementioned variation in the degrees of substrate-induced charging of the gold octamer deposited on magnesia surfaces with or without F-center defects (*33*). Indeed, ν(CO) for the complex bound to an F-center–rich surface is measured to be redshifted by 25 to 53 cm^{-1} with respect to the frequency of a CO molecule bonded to the complex deposited on an F-center–free support (Fig. 1). This compares favorably with the corresponding calculated red shift; for example, from Table 2, a value of 34 cm^{-1} is estimated when comparing ν(CO) for the C(FC-free) and B(FC) states [both corresponding to the complexes exhibiting the largest binding energy of the oxygen molecule (Table 2)].

We conclude that partial electron transfer from the F centers to the adsorbed cluster complex correlates with frequency shifts of the intramolecular vibration of adsorbed CO. In addition, these sites serve to strongly anchor the deposited clusters, thereby inhibiting their coalescence into larger inert ones. Understanding of such issues pertaining to the interactions between deposited clusters and the support surfaces, and investigations of the dependencies of such interactions on the materials' identity, their size, and their chemical and physical properties, promise to enhance progress toward the design and use of specific nanocatalytic systems.

References and Notes

1. M. Haruta, T. Kobayashi, H. Sano, N. Yamada, *Chem. Lett.* **34**, 405 (1987).
2. M. Haruta, *Catal. Today* **36**, 153 (1997).
3. M. Valden, X. Lai, D. W. Goodman, *Science* **281**, 1647 (1998).
4. A. Sanchez *et al.*, *J. Phys. Chem. A* **103**, 9573 (1999).
5. H. Häkkinen, S. Abbet, A. Sanchez, U. Heiz, U. Landman, *Angew. Chem. Int. Ed. Engl.* **42**, 1297 (2003).
6. M. Mavrikakis, P. Stoltze, J. K. Norskov, *Catal. Lett.* **64**, 101 (2000).
7. N. Lopez, J. K. Norskov, *J. Am. Chem. Soc.* **124**, 11262 (2002).
8. A. Cho, *Science* **299**, 1684 (2003).
9. C. Lemire, R. Meyer, S. Shaikhutdinov, H.-J. Freund, *Angew. Chem. Int. Ed. Engl.* **43**, 118 (2004).
10. J. Guzman, B. C. Gates, *J. Am. Chem. Soc.* **126**, 2672 (2004).
11. D. M. Cox, R. Brickman, K. Creegan, A. Kaldor, *Z. Phys. D* **19**, 353 (1991).
12. W. T. Wallace, R. L. Whetten, *J. Am. Chem. Soc.* **124**, 7499 (2002).
13. G. Mills, M. S. Gordon, H. Metiu, *Chem. Phys. Lett.* **359**, 493 (2002).
14. B. Yoon, H. Häkkinen, U. Landman, *J. Phys. Chem. A* **107**, 4066 (2003).
15. L. D. Socaciu *et al.*, *J. Am. Chem. Soc.* **125**, 10437 (2003).
16. D. Stolcic *et al.*, *J. Am. Chem. Soc.* **125**, 2848 (2003).
17. Y. D. Kim, M. Fischer, G. Ganteför, *Chem. Phys. Lett.* **377**, 170 (2003).
18. Details of the calculation methodology and comments about calculated vibrational frequencies are available on *Science* Online. The aforementioned theoretical ab initio predictions that charging plays a key role in the catalytic reactivity of gold clusters that are a few atoms in size has been clearly demonstrated recently through gas-phase studies. These investigations showed that only negatively charged even-numbered gold clusters bind a single O_2 molecule in a superoxo-like configuration (*16*, *17*) and that negatively charged free gold clusters are catalytically active for the CO-combustion reaction (*15*), whereas positively charged clusters are inert for the reaction, because oxygen cannot be adsorbed (*11*).
19. S. Abbet, K Judai, L Klinger, U. Heiz, *Pure Appl. Chem.* **74**, 1527 (2002).
20. A. S. Wörz, K. Judai, S. Abbet, U. Heiz, *J. Am. Chem. Soc.* **125**, 7964 (2003).
21. C. Ruggiero, P. Hollins, *J. Chem. Soc. Faraday Trans. 1* **92**, 4829 (1996).
22. P. Dumas, R. G. Tobin, P. L. Richards, *Surf. Sci.* **171**, 579 (1986).
23. Y. Jugnet, F. J. Cadete Santos Aires, C. Deranlot, L. Piccolo, J. C. Bertolini, *Surf. Sci.* **521**, L639 (2002).
24. D. R. Rainer, C. Xu, P. M. Holmblad, D. W. Goodman, *J. Vac. Sci. Technol. A* **15**, 1653 (1997).
25. C. Winkler, A. J. Carew, S. Haq, R. Raval, *Langmuir* **19**, 717 (2003).
26. U. Heiz, A. Sanchez, S. Abbet, W.-D. Schneider, *Chem. Phys.* **262**, 189 (2000).
27. R. N. Barnett, U. Landman, *Phys. Rev. B* **48**, 2081 (1993).
28. As discussed by us previously (*4*, *5*), for the adsorbed oxygen molecule, the transferred charge partially populates the antibonding orbital of the molecule, resulting for the systems studied here in increased interatomic distance $d(O_2)$, exhibiting characteristic superoxo (about 1.35 Å for $S = 1$; A and C in Table 2) and peroxo (about 1.42 Å for $S = 0$; B and D in Table 2) O–O distances, compared to a distance of 1.24 Å for the free molecule. The calculated stretch frequencies for the adsorbed O_2 molecule corresponding to the stronger binding states [B (for the F-center–rich surface) and C (for the F-center–free surface) (Table 2)] are 966 and 1084 cm^{-1}, respectively. For reference, we note that for free O_2 we obtained a frequency of 1485 cm^{-1} as compared to the experimental value of 1580 cm^{-1}. Because the peripherially adsorbed O_2 is oriented parallel to the surface (Fig. 2F), it is IR-inactive. The aforementioned measured IR absorption band (at 1300 cm^{-1}) originates from IR-active configurations of O_2 molecules [for example, the ensemble of supported Au_8 clusters with the molecule adsorbed on the top facet of the cluster (*4*)].
29. The consequent depletion of the 5σ frontier orbital is often referred to in surface science studies as (forward) donation from CO to the metal (*30*, *31*).
30. G. Blyholder, *J. Phys. Chem.* **68**, 2772 (1964).
31. R. Hoffmann, *Rev. Mod. Phys.* **60**, 601 (1988).
32. L. Lian, P. A. Hackett, D. M. Rainer, *J. Chem. Phys.* **99**, 2583 (1993).
33. The binding energy of the molecule to the gold cluster is the result of several factors that manifest themselves simultaneously (the aforementioned hybridizations of the CO 5σ and 1π orbitals with the *s-d* wavefunctions of the gold cluster, in addition to the contribution to the binding associated with population of the $2\pi^*$ orbital). Consequently, although the C–O bond length and the CO vibrational frequency are sensitive to and correlate with the degree of back-donation into the hybridized antibonding $2\pi^*$ orbital, the adsorption energy of CO to the gold cluster may not exhibit such correlation (for example, results in Table 2).

34. U.L., B.Y., and H.H. acknowledge support by the U.S. Air Force Office of Scientific Research and the U.S. Department of Energy (DOE). The computer simulations were performed on U.S. Department of Defense computers supported by the High Performance Computing Modernization Program and at DOE's National Energy Research Scientific Computing Center at the Lawrence Berkeley National Laboratory. The experiments were carried out at the University of Ulm. Support for the experiments was also obtained from the Deutsche Forschungsgemeinschaft, the Sonderforschungsbereich 569, and the Landesstiftung Baden-Württemberg. K.J. thanks the Alexander v. Humboldt foundation and the Japan Society for the Promotion of Science foundation for financial support, J.-M.A. thanks the Swiss National Science foundation, and S.A. thanks the Alexander v. Humboldt foundation for financial support. A.S.W. acknowledges support from the Graduiertenkolleg Molekulare Organisation und Dynamik an Grenz- und Oberflächen.

Supporting Online Material

www.sciencemag.org/cgi/content/full/307/5708/403/DC1
SOM Text
References

17 August 2004; accepted 30 November 2004
10.1126/science.1104168